Available online at www.sciencedirect.com
ScienceDirect
Journal of Photochemistry and Photobiology A: Chemistry 194 (2008) 152–160
Journal of Photochemistry and Photobiology A:Chemistry
www.elsevier.com/locate/jphotochem

Preparation of high efficient photoelectrode of N–F-codoped TiO_2 nanotubes

Yaling Su, Xingwang Zhang, Minghua Zhou, Song Han, Lecheng Lei *

Institute of Environmental Pollution Control Technologies, Xixi Campus, Zhejiang University, Hangzhou 310028, PR China

Received 27 January 2007; received in revised form 8 July 2007; accepted 1 August 2007
Available online 6 August 2007

Abstract

In order to obtain TiO_2 electrode with high photoelectrocatalytic activity, a novel N–F-codoped TiO_2 nanotubes electrode was prepared by electrochemical anodization of Ti in $C_2H_2O_4{\cdot}2H_2O + NH_4F$ electrolyte. The prepared electrode had a highly self-organized structure with high-specific surface area, and N and F were successfully doped into the lattice of TiO_2. When voltage during anodization was 20 V, annealing temperature was 673 K and anodic bias potential in the photoelectrocatalytic degradation was 0.25 V, N–F-codoped TiO_2 nanotubes electrode showed the higher catalytic activity. In addition, there was an obvious synergetic effect between the electrochemical and photocatalytic processes, and the synergetic factor *R* reached 8.7. This high-synergetic effect was attributed to the advantages of photoelectrocatalytic technique using high-aspect-ratio TiO_2 nanotubes and the promoting effect of N–F-codoping on the catalytic activity. Moreover, N–F-codoped TiO_2 nanotubes electrode showed good stability and after five times the photoelectrocatalytic efficiencies of MO still kept above 97% within 80 min.

Keywords: TiO_2 nanotubes electrode; N–F-codoping; Anodization; Photoelectrocatalysis

1. Introduction

TiO_2 is considered to be the most attractive photocatalyst due to its high oxidative power, photostability, low cost and nontoxicity [1]. However, a major problem baffling the application of TiO_2, not yet fully overcome, is the recombination of the photogenerated charge carriers during the photocatalytic process. Two important approaches were studied to solve this problem. One promising strategy is the application of electrical bias, using an external counter electrode, to inhibit the recombination of electrons and holes and the lifetime of photogenerated carriers remains long. This photoelectrocatalytic technique combines UV illumination with the application of a controlled potential through a supported catalyst, thus its efficiency is much higher than that of the single photocatalytic process [2–5]. The other approach is nonmetal doping such as F-doping [6,7] and Cl–Br-codoping [8] of TiO_2. For example, the doped F atoms can convert Ti^{4+} to Ti^{3+} by charge compensation and that the presence of a certain amount of Ti^{3+} reduces the electron–hole recombination rate and thus enhances the photocatalytic activity [7]. Consequently, developing a novel nonmetal-doped TiO_2 photoelectrode has a significant interest.

Since the first TiO_2 photoelectrocatalytic oxidation study for degrading 4-chlorophenol in aqueous solutions was carried out by Vinodgopal et al. [2], numerous studies were carried out for organic pollutants by photoelectrocatalytic technology, such as chlorophenols, dyes, detergent and organic acids under UV light irradiation [2,9–12]. Generally, in these studies, photoanodes were TiO_2 film electrodes. However, the specific surface area of TiO_2 film electrodes was commonly low and as a result, their photoelectrocatalytic activity was low. In fact, it is on the TiO_2 surface that different types of radicals are formed to promote the degradation reaction. Therefore, the specific surface area has a significant effect on the catalytic activity of TiO_2 electrode.

Presently, TiO_2 nanotubes are gaining extraordinary interest for their high-specific surface area. This novel supported tubular structure of TiO_2 is a promising electrode for application in photoelectrocatalytic process. TiO_2 nanotubes of different geometrical shapes and microstructures in powder forms have been prepared by different techniques such as sol–gel synthesis [13], freeze-drying [14], electrodeposition [15], sonochemical

* Corresponding author. Tel.: +86 571 88273090; fax: +86 571 88273693.
E-mail address: lclei@zju.edu.cn (L. Lei).

1010-6030/$ – see front matter © 2007 Elsevier B.V. All rights reserved.
doi:10.1016/j.jphotochem.2007.08.002

deposition [16] and chemical treatments of fine titania particles [17,18]. However, TiO_2 nanotubes obtained by these methods are unfit for being used as working electrodes in photoelectrocatalytic degradation of pollutants because of their powder forms.

As an effective preparation technology, the electrochemical anodization method shows its advantage on preparing an integrative electrode with an immobilization TiO_2 nanotubes [19–21], which possesses good mechanical adhesion strength and electronic conductivity because it is directly grown from titanium metal substrate. Moreover, the thickness and morphology of such TiO_2 nanotubes are easily controlled by regulating the electrolyzing conditions such as anodization time and electrolyte composition [22,23].

In addition, it was reported that N-doped TiO_2 nanotubes can be obtained by using heat treatment in ammonia [24] or by ion implantation [25], and they showed some photoresponse under visible light. However, ammonia gas is hazardous, and ion implantation process is complicated and leads to a certain decrease of photoresponse in the UV range [25]. Consequently, it is in need of developing a novel nonmetal-doping approach to avoid decrease of photoresponse in the UV range. In fact, the introduction of fluorine atoms into TiO_2 is also effective for enhancing the photocatalytic activity of TiO_2 under UV irradiation [6]. Moreover, N–F-codoping of TiO_2 presented an obvious synergetic effect and further enhanced its photocatalytic activity. This seems to be a consequence of the perfect combination of some beneficial effects induced by both N and F dopants. N-doping into TiO_2 resulted in the creation of surface oxygen vacancies, and F-doping produced several beneficial effects, including the creation of surface oxygen vacancies, the enhancement of surface acidity and the Ti^{3+} ions [7]. This synergetic effect can promote the separation of photogenerated carriers, and thus the photocatalytic reaction under UV irradiation can be accelerated. Therefore, it is interesting to explore the possibility to prepare N–F-codoped TiO_2 nanotubes electrode by a simple and efficient process, and its photoelectrochemical activity needs research.

In the present work, the objective was to prepare N–F-codoped TiO_2 nanotubes electrode with high efficiency under UV irradiation by one-step anodization process, integrating preparation with doping by adjusting the electrolyte composition. NH_4F is beneficial to obtain high-aspect-ratio TiO_2 nanotubes as buffered species [26]. Organic solvents can avoid nanotubes breakdown caused by high current density due to their high resistivity [27]. Therefore, oxalic acid ($C_2H_2O_4{\cdot}2H_2O$) + NH_4F electrolyte was selected in this work to prepare N–F-codoped TiO_2 nanotubes electrode by anodization. $C_2H_2O_4{\cdot}2H_2O$ was ever successfully used to fabricate nanoporous anodic aluminum oxide by electrochemical anodization [28]. And in this work, the other more important role of NH_4F is that this species can offer N and F to dope TiO_2 nanotubes [6]. The N–F-codoped TiO_2 nanotubes electrode was characterized and its formation mechanism and process of N- and F-doping was discussed. Finally, its photoelectrocatalytic activity was evaluated by the photoelectrodegradation of an azo compound, methyl orange (MO).

2. Experimental

2.1. Sample preparation

The high purity titanium sheet (99.60% purity) was obtained from Haiji Ltd. for Titanium & Nickel (Shannxi, China.). NH_4F and $C_2H_2O_4{\cdot}2H_2O$ were of analytical grade. All compounds were used as received without further purification. The titanium sheet was first mechanically polished with abrasive papers, washed in an ultrasonic bath with distilled water and acetone, and then dried in air at room temperature. Electrochemical experiments were conducted using a direct current (dc) power supply (QJ3003A, Zhongce Electronical Co. Ltd., Hangzhou, China). Titanium sheet served as anodic electrode and nickel sheet as the cathode. The electrolyte was 1/12 M $C_2H_2O_4{\cdot}2H_2O$ + 0.5 wt.% NH_4F aqueous solution, and anodization voltages of 10 V, 20 V and 30 V were respectively used in the present work. All the anodization experiments were carried out at room temperature with magnetic agitation. After the anodization, the color of the titanium sheet surface was yellowish and the samples were rinsed in deionized water and dried.

2.2. Characterization

For a morphology characterization of N–F-codoped TiO_2 nanotubes electrode, a field-emission scanning electron microscopy (FE-SEM, JSM-5600LV) was used.

The crystal structure of the samples was identified by X-ray diffraction (XRD, Rigaku, D/max-rA) using a diffractometer with Cu Kα radiation, performed over angular ranges of $2\theta = 20–80^\circ$, scanned at a speed of 0.02°/s and steps of 0.02°. The equipment was operated at 40 kV and 80 mA.

The elemental composition of N–F-codoped TiO_2 nanotubes electrode was determined by X-ray photoelectron spectroscopy (XPS, Perkin-Elmer, a RBD upgraded PHI-5000C ESCA system) with Mg Kα radiation ($h\nu = 1253.6$ eV), the X-ray anode was run at 250 W and the high voltage was kept at 14.0 kV with a detection angle at 54°.

For investigating the mechanism of the formation of N–F-codoped TiO_2 nanotubes electrode, current–time transient of Ti in electrolyte was recorded by electrochemical station (Shanghai ChenHua, CHI600B).

2.3. Photoelectrocatalytic degradation of MO solution

The effectiveness of N–F-codoped TiO_2 nanotubes electrode was evaluated by the degradation of MO solution. The chemical structure of methyl orange is:

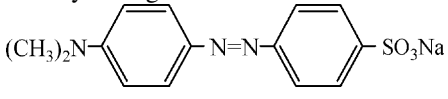

The experiment was performed in a 1.5 L cylindrical glass reactor, with an ultraviolet (UV) irradiation (a 300 W high-pressure mercury lamp from Shanghai YaMing Light with a maximum wavelength of 365 nm, $I_0 = 0.6$ mW/cm^2), vertically inserted in a central quartz glass cannula, as shown in Fig. 1. The initial concentration of MO was 10 mg/L, adding 0.1 M sodium

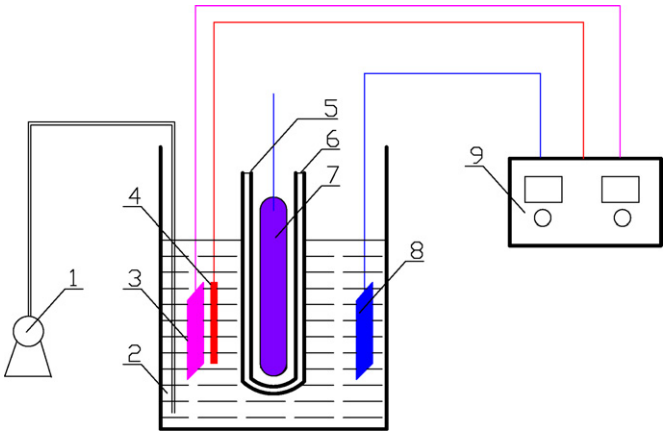

Fig. 1. Schematic diagram of photoelectrocatalytic reactor ((1) air compressor; (2) MO solution; (3) working electrode (TiO_2/Ti); (4) reference electrode; (5) inlet of cooling water; (6) outlet of cooling water; (7) high-pressure mercury lamp; (8) counter electrode (nickel sheet); (9) potentiostat).

sulfate as electrolyte. The counter electrode was nickel sheet. The concentration of MO was monitored by a TECHCOMP 8500 spectrophotometer (463 nm). The removal (within 80 min) is calculated as $[1-(C/C_0)\times 100\%]$, where C_0 is the initial concentration of MO and C is the concentration of MO during reaction. Moreover, the synergetic factor R was introduced to evaluate the synergetic effect by comparing the apparent rate constants (k_{app}) of degradation of MO in photoelectrocatalytic (PEC), photocatalytic (PC) and electrochemical (EC) processes.

$$R = \frac{k_{app}\text{ of MO degradation in PEC process}}{k_{app}\text{ of MO degradation in PC process} + k_{app}\text{ of MO degradation in EC process}}$$

3. Results and discussion

3.1. Characterization of N–F-codoped TiO_2 nanotubes electrode

Fig. 2a–c shows SEM images of N–F-codoped TiO_2 nanotubes electrode formed at 10 V, 20 V and 30 V for 0.5 h, respectively, in 1/12 M $C_2H_2O_4{\cdot}2H_2O$ + 0.5 wt.% NH_4F electrolyte. It was obvious that the inner diameter of N–F-codoped TiO_2 nanotubes electrode formed at 10 V was approximately 28 nm, and that of the sample formed at 20 V was in the range of 35–55 nm. However, the nanotubular structure of the sample formed at 10 V was not such visible and self-organized as that of the sample formed at 20 V. In addition, a sponge-like porous structure was formed at 30 V, and the pore size was larger and no obvious nanotubular structure appeared. This revealed that the diameter of N–F-codoped TiO_2 nanotubes electrode increased with the anodization voltage, and its surface morphology were

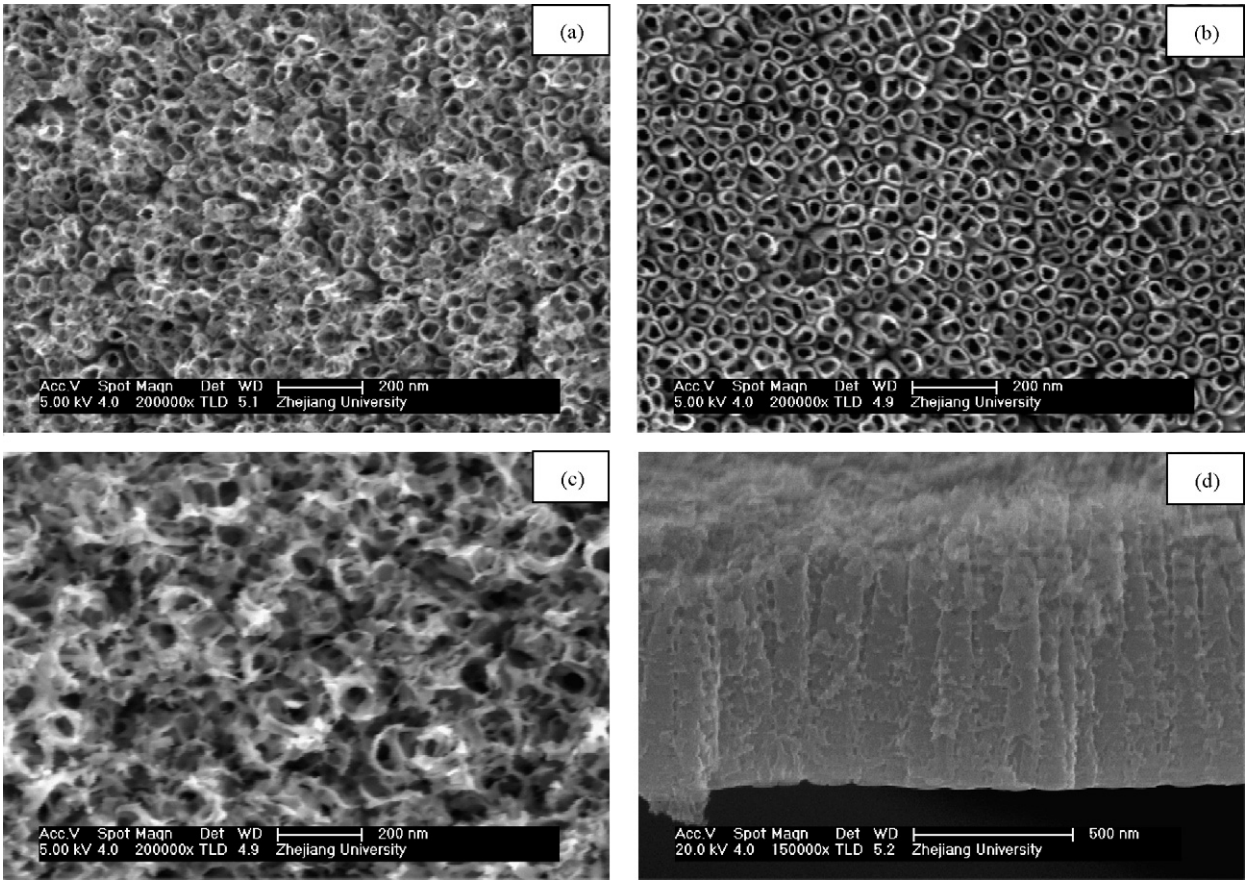

Fig. 2. SEM images of N–F-codoped TiO_2 nanotubes electrode anodized in 1/12 M $C_2H_2O_4{\cdot}2H_2O$ + 0.5 wt.% NH_4F at anodization voltages of 10 V (a), 20 V (b), 30 V (c) and cross-sectional images of the sample anodized at 20 V (d).

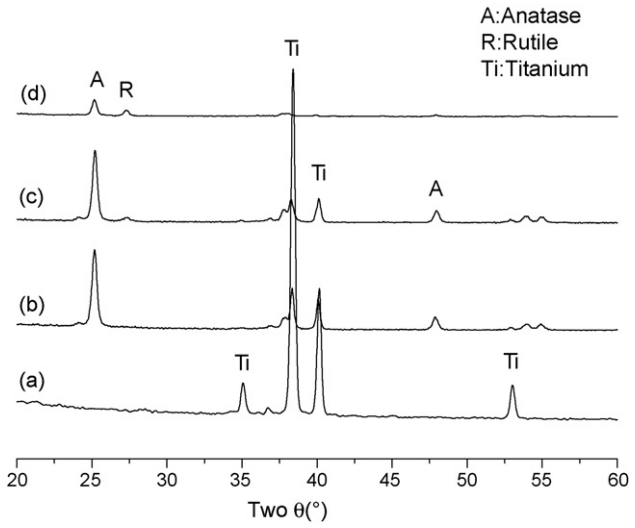

Fig. 3. XRD patterns of N–F-codoped TiO_2 nanotubes electrode before annealing (a), after annealing at 673 K (b), 773 K (c) and 873 K (d), respectively, for 2 h in an air atmosphere.

also greatly depend on the anodization voltage. Fig. 2d presented the cross-sectional image of the sample anodized at 20 V for 0.5 h. It was clear that the length of the nanotubes was in the range of 800–900 nm. It should be noted that the nanotubes in this work had the smaller inner diameter and the longer length than the nanotubes prepared in HF electrolyte [29]. This was possible for the lower current density in $C_2H_2O_4{\cdot}2H_2O$ solution with high resistivity.

Fig. 3 depicts XRD patterns of TiO_2 nanotubes electrode before and after annealing at 673 K, 773 K and 873 K for 2 h in an air atmosphere, respectively. It was seen that the amorphous phase was dominant before annealing, and anatase TiO_2 ($2\theta = 25.3^\circ$) was obtained after annealing at 673 K and a mixture of rutile ($2\theta = 27.3^\circ$) and anatase phase appeared after annealing at 773 K and 873 K. The peak at 25.3° was the diffraction of (1 0 1) of anatase and the peak at 27.5° was the diffraction of (1 1 0) of rutile. This indicated that the annealing temperature had a great effect on the phase composition of TiO_2 nanotubes electrode. However, it should be noted that the intensity of diffraction peak corresponding to rutile TiO_2 appeared in the sample annealed at 773 K was obviously stronger than that appeared in the sample annealed at 873 K, indicating the larger amount of rutile phase. In addition, there are no diffraction peaks corresponding to other TiO_2 crystals.

The elemental composition of N–F-codoped TiO_2 nanotubes electrode was determined by XPS. The sample was anodized at 20 V for 0.5 h in 1/12 M $C_2H_2O_4{\cdot}2H_2O$ + 0.5 wt.% NH_4F electrolyte, and annealed at 673 K for 2 h in an air atmosphere. Fig. 4a shows that the prepared electrode consists of Ti, O, C, N and F. The atomic concentration of Ti, O and C was 21.10 at.%, 51.65 at.% and 25.25 at.%, respectively. The atomic ratio of Ti/O was above 1:2. It is very much likely that the oxygen excess is associated with the carbon. The C element was mainly ascribed to the adventitious hydrocarbon from XPS itself. The residual carbon from electrolyte and adventitious element carbon may also cause the presence of C element [30]. It should be noted that the concentrations of total-N and total-F in TiO_2 nanotubes were 0.72 at.% and 1.28 at.%, respectively. The chemical forms of the N/F atoms in TiO_2 nanotubes were investigated from the analysis of the high-resolution XPS spectra.

Fig. 4b depicts two peaks of binding energy of N 1s of 396.25 eV and 401.9 eV, respectively. The peak at 396.25 eV was generally considered as the evidence for the presence Ti–N bonds formed when N atoms replace the oxygen in TiO_2 crystal lattice. Here, these N atoms are called site-N. This is possible because N 2p states can mix with O 2p states, and thus N atoms substitute O atoms in the TiO_2 crystal lattice. The peak at 401.9 eV could pertain to N atoms from adventitious N_2 or NH_3 adsorbed on the surface of TiO_2 [31].

Fig. 4c shows the high-resolution XPS spectra of F 1s. It was observed that an unsymmetrical F 1s peak. This means that different chemical forms of F atoms might exist in TiO_2 nanotubes electrode. Therefore, the F 1s peak was deconvoluted into two separated peaks with Gaussian distributions. The peak at 686.4 eV of F 1s was originated from the F atoms of the $TiOF_2$ [7]. The peak at 688.5 eV could pertain to Ti–F bonds [32,33], that is, the substitutional F atoms that occupied oxygen sites in the TiO_2 crystal lattice, and the position of this peak was close to the value reported by Yu for the substitutional F atoms in TiO_2 [6]. These results indicated that the F atoms were also doped into TiO_2 nanotubes electrode. This is understandable because the ionic radius of 0.136 nm for F^- is equal to that of 0.140 nm for O^{2-}, resulting in F^- to substitute O^{2-}.

Fig. 4d shows that the XPS spectra of Ti $2p_{3/2}$ in TiO_2. It could be fitted as one peak at 460.4 eV, indicating that Ti ions were mainly in an octahedral environment and its valence state was not influenced by a small amount of doping, and a trace of Ti^{3+} was not detected. Meanwhile, the binding energy of Ti $2p_{3/2}$ of 460.4 eV was larger than that of the standard value (458 ± 0.1 eV) [34], which meant that the surface acidity of TiO_2 was enhanced, and thus it was easy for the polar organic pollutants to be adsorbed on the catalyst surface. The XPS spectra of the O 1s region were also taken, as shown in Fig. 4e. The O 1s region could be fitted by four peaks at 530.9 eV, 531.8 eV, 533.0 eV and 534.6 eV, corresponding to the Ti–O bond in TiO_2, hydroxyl groups on the surface, oxygen chemically adsorbed on the surface and H_2O molecule adsorbed on the surface [35,36].

3.2. Formation mechanism of N–F-codoped TiO_2 nanotubes electrode

3.2.1. Formation of TiO_2 nanotubes electrode

For investigating into the formation mechanism of N–F-codoped TiO_2 nanotubes electrode, current–time transient of Ti in electrolyte was recorded. Fig. 5 shows that during the anodization, N–F-codoped TiO_2 nanotubes are formed through three phases. In comparison with the result reported by Lai et al. [37], the current–time transient in this work was much slower. This can be attributed to the higher resistivity in

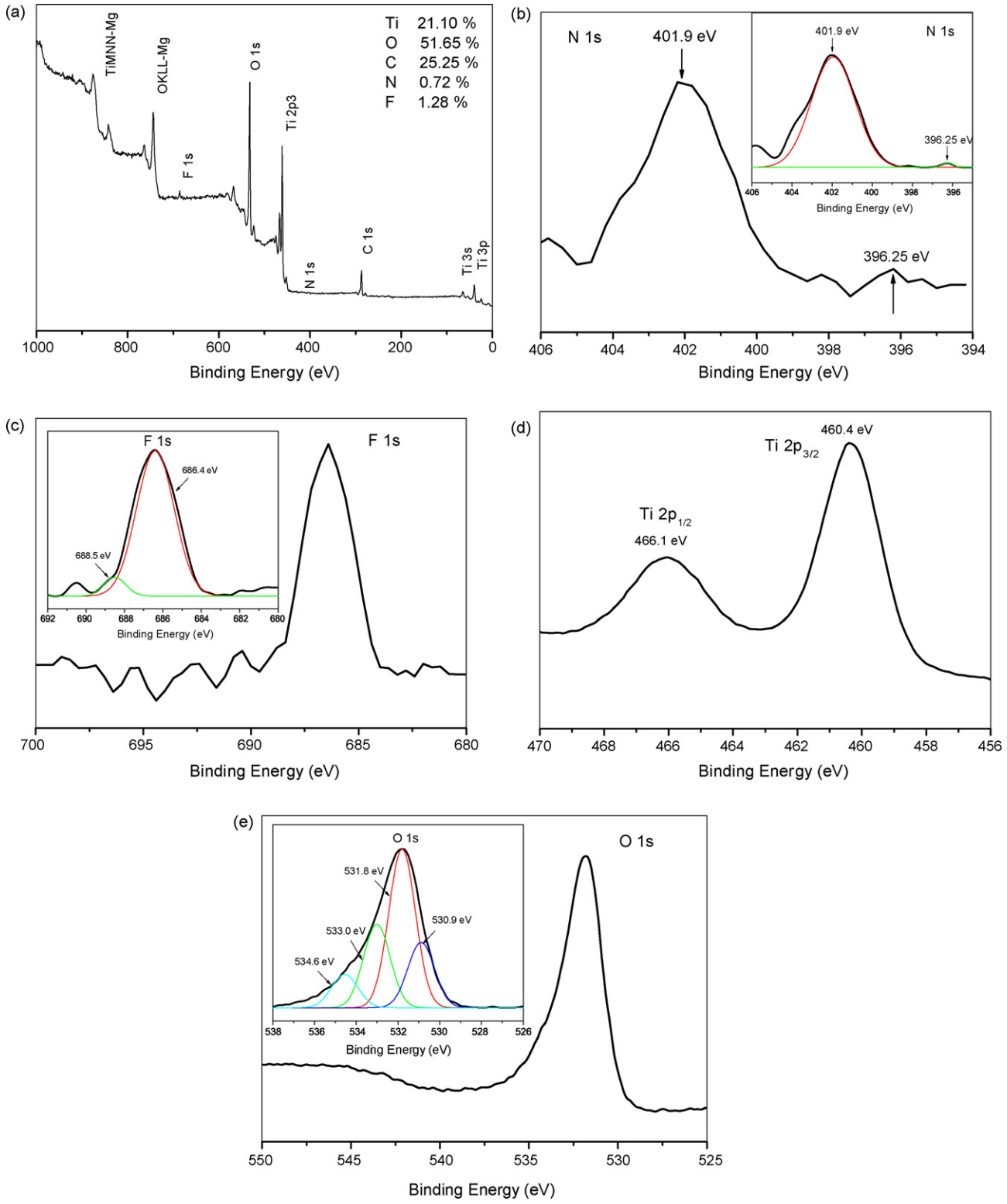

Fig. 4. The whole XPS spectra (a), N 1s XPS spectra (b), F 1s XPS spectra (c), Ti 2p XPS spectra (d) and O 1s XPS spectra (e) of N–F-codoped TiO_2 nanotubes electrode.

$C_2H_2O_4{\cdot}2H_2O + NH_4F$ electrolyte than that in HF electrolyte. In the initial phase, titanium dissolved rapidly in electrolyte and thus anode current was very large. Then large numbers of Ti^{4+} came into being and immediately reacted with ions containing oxygen to form a compact barrier layer of TiO_2 film, and current decreased sharply. An oxide layer initially formed via the following reactions [38]:

$$2H_2O \rightarrow O_2 + 4e^- + 4H^+ \quad (1)$$

$$Ti + O_2 \rightarrow TiO_2 \quad (2)$$

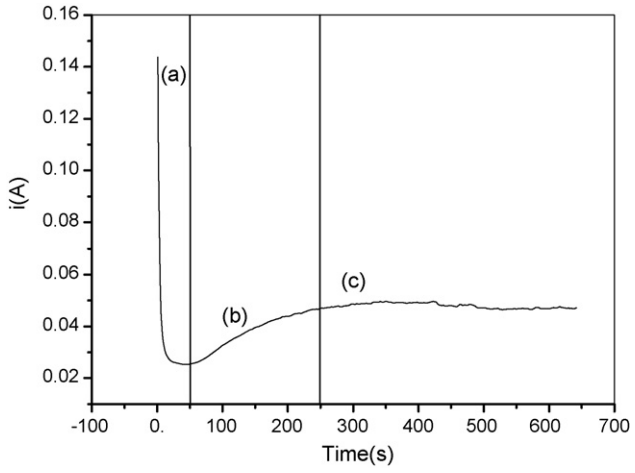

Fig. 5. Current–time transient of Ti in 1/12 M $C_2H_2O_4{\cdot}2H_2O$ + 0.5 wt.% NH_4F electrolyte.

Then the second phase began, electric field intensity increased rapidly with the formation of oxide layer. Under the combined effect of electric field and electrolyte, the barrier layer of TiO_2 film dissolved to form cores of porous layer, which gradually became to form pores distributed highly self-organized. The pores were the result of the localized chemical dissolution of the oxide by F^-. In this phase, Ti^{4+} could easily traverse the barrier layer to go into the solution, and ions containing oxygen in the solution could also easily traverse the barrier layer to react with Ti^{4+}. Therefore, a new barrier layer was formed and current rose.

In the third phase, porous layer grew steadily. Current was generated from ions transferring in both sides of the barrier layer and kept a steady-state value. The oxide layer in the bottom of pores grew continuously toward inside of the titanium sheet. When the growing speed at barrier–titanium interface was equal to the dissolved speed of the oxide layer in the bottom, the barrier layer stopped growing inside. Finally, N–F-doped TiO_2 nanotubes electrode with a constant length were formed.

3.2.2. Processes of N- and F-doping of TiO_2 nanotubes electrode

Different processes of the N- and F-doping were considered. The N-doping into the TiO_2 crystal lattice occurred following the NH_4F decomposition into NH_3 and proceeded through the following reaction:

$$TiO_2 + NH_3 \rightarrow TiO_{2-x}N_x + H_2O \quad (3)$$

The process of F-doping into the TiO_2 crystal lattice is presented by reactions (4) and (5). First, TiO_2 reacted with F^-, from dissolution of NH_4F, to form TiF_6^{2-}. Then during the TiF_6^{2-} hydrolysis, part of the Ti–F bonds did not break and directly remained in the TiO_2 crystal lattice:

$$TiO_2 + 6F^- + 4H^+ \rightarrow TiF_6^{2-} + 2H_2O \quad (4)$$

$$TiF_6^{2-} + 2H_2O \rightarrow TiO_{2-y}F_y + HF + NH_3 \quad (5)$$

3.3. Photoelectrocatalytic activity evaluation

3.3.1. Effect of voltages during anodization

N–F-codoped TiO_2 nanotubes electrodes anodized at different anodization voltages were tested to compare their photoelectrocatalytic efficiencies by MO degradation. All samples were annealed at 673 K after anodization and 0.25 V (versus SCE) of anodic bias potential was applied. It is well recognized that the photoreaction generally fits with the Langmuir–Hinshlwood kinetics expression with the rate being proportional to the coverage θ [39]:

$$r = k\theta = \frac{kKC}{1 + KC}$$

where k is the true rate constant which includes various parameters such as the mass of catalyst, the flux of efficient photons, the coverage in oxygen, etc., and K is the adsorption constant. When the initial concentration is very low (10 mg/L), the term KC in the denominator can be neglected with respect to unity and the rate becomes, apparently, first order:

$$r = -\frac{dC}{dt} = kKC = k_{app}C$$

where k_{app} is the apparent rate constants of pseudo-first-order. The integral form of the rate equation is

$$\ln \frac{C_0}{C} = k_{app}t$$

The apparent rate constants (k_{app}) was calculated from the slopes of ln(concentration versus time). In this research, pseudo-first-order kinetics was also confirmed in the photoelectrocatalytic process of MO. The apparent rate constants and regression coefficients are presented in Table 1. It was seen that the sample anodized 20 V had the higher apparent rate constant (k_{app}), indicating the higher photoelectrocatalytic activity. In fact, these SEM images indicated that N–F-codoped TiO_2 nanotubes anodized at 20 V had a more distinct and self-organized tubular structure, and thus had the higher specific surface area than that anodized at 10 V and 30 V, which could adsorb more MO molecules to be excited by UV irradiation to produce more activated states for degradation.

3.3.2. Effect of annealing temperature

The effect of annealing temperature on the photoelectrocatalytic efficiency was investigated. The apparent rate constants and regression coefficients of N–F-codoped TiO_2 nanotubes annealed at 673 K, 773 K and 873 K are also shown in Table 1. Samples were anodized at 20 V and 0.25 V (versus SCE) of anodic bias potential was applied. It was apparent that N–F-codoped TiO_2 nanotubes (673 K) had the higher degradation rate of MO among the samples. Actually, these results of XRD patterns indicated anatase TiO_2 was entirely obtained after annealing at 673 K, and a mixture of rutile and anatase phase appeared after annealing at 773 K and 873 K. Generally, anatase TiO_2 showed excellent photoactivity in photocatalytic reaction due to its high-specific surface area, strong adsorption for oxygen [2,9–12]. Meanwhile, some research revealed that rutile

Table 1
The kinetic constants and regression coeffcients of the degradation of MO

Anodization voltage (V)	Annealing temperature (K)	Oxidation process	Anodic bias (vs. SCE) (V)	Kinetic constants k_{app} (min^{-1})	Regression coefficients R^2
10[a]	673	PEC	0.25	0.04381	0.9938
20[a]	673	PEC	0.25	0.07066	0.9712
30[a]	673	PEC	0.25	0.04798	0.9933
20[a]	773	PEC	0.25	0.04745	0.9681
20[a]	873	PEC	0.25	0.03245	0.9985
20[a]	673	PC	–	0.00782	0.9654
20[a]	673	EC	0.25	0.00030	0.9658
–	–	DP	–	0.00632	0.9922
20[b]	673	PEC	0.25	0.04323	0.9449

[a] The sample was anodized in $C_2H_2O_4{\cdot}2H_2O + NH_4F$ electrolyte.
[b] The sample was anodized in HF electrolyte.

TiO_2 photoelectrode also showed photoactivity to a certain extent [39–41]. In this study, anatase TiO_2 had a higher photoelectrocatalytic activity, in accordance with the conclusions in most published work.

3.3.3. Effect of anodic bias potential on MO degradation

In order to investigate the effect of anodic bias potential on MO degradation, linear sweep voltammetry was conducted. Fig. 6 shows the voltammograms of MO with and without UV illumination. When the potential was below +0.25 V, the rate of photoelectron transport process was lower and controlled the overall PEC oxidation. The applied bias resulted in the increase of space charge layer and band bending, thus promoted the separation of photogenerated carriers and interface charge transfer rate of TiO_2/solution. Thus, the photocurrent increased in the range of 0–0.25 V. Once the anodic bias exceeded +0.50 V, under given light intensity, the photogenerated carriers were fully separated, which leads to saturated photocurrent and the rate increases slowly. Under this condition, the interfacial oxidation became the rate-determining step of the overall process, and its rate was slower than the photoelectron transport [41–43].

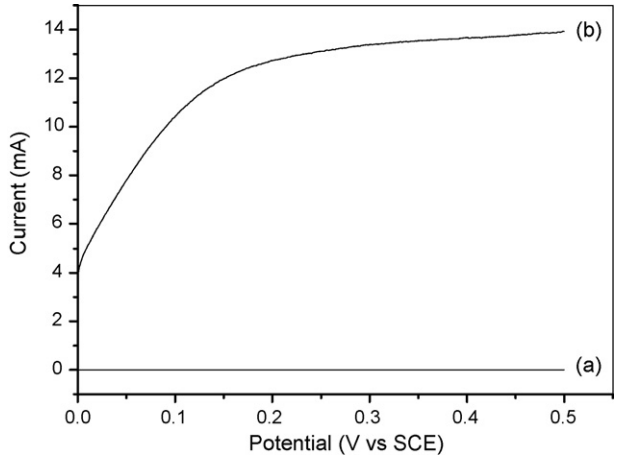

Fig. 6. Current–potential curves at N–F-codoped TiO_2 nanotubes electrode with and without UV irradiation in 0.1 M Na_2SO_4 containing 10 mg/L MO: (a) in the dark and (b) under UV irradiation. The sample were anodized at 20 V and annealed at 673 K.

3.3.4. Comparison among EC, PC and PEC processes of MO

The apparent rate constants and regression coefficients of the electrochemical (EC), photocatalytic (PC), photoelectrocatalytic (PEC) and direct photolysis (DP) processes of MO were presented in Table 1. For comparison, the photoelectrocatalytic activity of the only-F-doped TiO_2 nanotubes electrode prepared in HF electrolyte was tested. In this work, note that only-N-doped and un-doped TiO_2 nanotubes electrodes were not prepared because generally the electrolyte should contain F^- during anodization. All samples were anodized 20 V and annealed 673 K and 0.25 V of anodic bias potential was applied in electrochemical and photoelectrocatalytic processes. It was seen from Table 1 that the direct photolysis of MO under UV illumination was proven to be present. Comparing with N–F-codoped TiO_2 nanotubes electrode, the photoelectrocatalytic activity of only-F-doped electrode was lower, indicating the promoting effect of N and F on the separation of photogenerated carriers, which accelerated the photocatalytic reaction under UV irradiation. Moreover, these results indicated that there was an obvious synergetic effect between the EC and PC processes, and the synergetic factor R in this work reached 8.7. As we know, under UV excitation, anodic bias potential can drive the photogenerated electrons to the counter compartment via the external circuit, and the photogenerated holes quickly move in opposite directions of the electrons to accumulate on TiO_2 nanotubes surface, thus their recombination is greatly suppressed. The holes that remain on the TiO_2 nanotubes are efficiently utilized in the oxidation of the dye molecules and the photocatalytic efficiency is improved [2]. Moreover, the higher specific surface area of TiO_2 nanotubes favors adsorbing more dye molecules to be oxidized. In addition, the promoting effect of N–F-codoping has also a contribution to the higher synergetic effect in this study. As above mentioned, N-doping into TiO_2 resulted in the creation of surface oxygen vacancies, and F-doping produced several beneficial effects, including the creation of surface oxygen vacancies, the enhancement of surface acidity and the Ti^{3+} ions. As a result, the promoting effect was induced by both N and F dopants [7]. The presence of Ti^{3+} ions reduces the electron–hole recombination rate and thus enhances the photocatalytic activity [6].

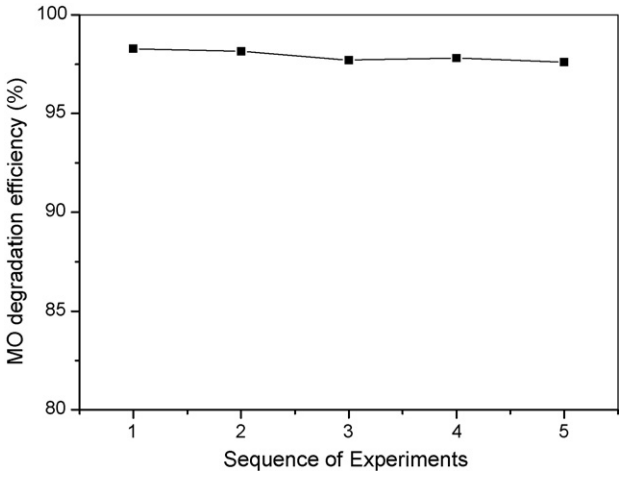

Fig. 7. MO photoelectrocatalytic degradation efficiencies of five repeated experiments with N–F-codoped TiO_2 nanotubes electrode (20 V, 673 K) (experiment condition: 10 mg/L initial concentration of MO, 0.1 M Na_2SO_4, 0.25 V anodic bias potential, 80 min irradiation time).

3.3.5. Stability of N–F-codoped TiO_2 nanotubes electrode

The stability of N–F-codoped TiO_2 nanotubes electrode was investigated five times by repeating photoelectrocatalysis degradation of MO, as shown in Fig. 7. N–F-codoped TiO_2 nanotubes electrode was cleaned with ultrasonication after each experiment. It was interesting to find that after five repeated experiments for photoelectrocatalytic degradation of MO for 80 min, the degradation efficiencies were rather stable and still kept above 97%.

4. Conclusions

The high efficient photoelectrode of N–F-codoped TiO_2 nanotubes electrode was prepared by electrochemical anodization of Ti in $C_2H_2O_4{\cdot}2H_2O + NH_4F$ electrolyte. The diameter of N–F-codoped TiO_2 nanotubes electrode increased with the anodization voltage, and its surface morphology of nanotubes electrode were also greatly depend on the anodization voltage. The optimum value of anodization voltage was 20 V.

During anodization, nitrogen and fluorine was successfully doped TiO_2 nanotubes electrode by one-step process, integrating preparation with doping. N–F-codoped TiO_2 nanotubes are formed through three phases: the formation of TiO_2 film oxide layer; the formation of porous layer; the stead growth of porous layer. Meanwhile, the N-doping into the TiO_2 crystal lattice occurred following the NH_4F decomposition into NH_3; and the process of F-doping into the TiO_2 crystal lattice undergo two steps: TiO_2 first reacted with F^- to form TiF_6^{2-}, then during the TiF_6^{2-} hydrolysis, part of the Ti–F bonds did not break and directly remained in the TiO_2 crystal lattice.

N–F-codoped TiO_2 nanotubes electrode showed the higher photoelectrocatalytic activity under the following conditions: voltage during anodization was 20 V, annealing temperature was 673 K and anodic bias potential was 0.25 V. It was worthy to be noted that there was an obvious synergetic effect between the electrochemical process and the photocatalytic process. The synergetic factor *R* reached 8.7. The obvious synergetic effect was attributed to the advantages of photoelectrocatalytic technique using high-aspect-ratio TiO_2 nanotubes and the promoting effect of N–F-codoping on the catalytic activity. Moreover, N–F-codoped TiO_2 nanotubes electrode showed good stability and after five repeated experiments the photoelectrocatalytic efficiencies of MO still kept above 97% within 80 min.

Acknowledgements

This project was supported by the National Science Foundation of China (nos. 20676121, 90610005 and 20336030) and China Postdoctoral Science Foundation (no. 20060400319). The authors would like to acknowledge Dr. Wang for his help with the SEM analysis. We also express our appreciation to Dr. Hu for her great assistance with XRD analysis and to Prof. Dai for XPS analysis.

References

[1] A.L. Linsebigler, G.Q. Lu, T. Yates Jr., Chem. Rev. 95 (1995) 735–758.
[2] K. Vinodgopal, S. Hotechandani, P.V. Kamat, J. Phys. Chem. 97 (1993) 9040–9044.
[3] D.H. Kim, M.A. Anderson, Environ. Sci. Technol. 28 (1994) 479–483.
[4] R. Pelegrini, P. Perqlta-Zamora, A.R. Andrade, J. Reyes, Appl. Catal. B: Environ. 22 (1999) 83–90.
[5] M.V.B. Zanoni, J.J. Sene, M.A. Anderson, J. Photochem. Photobiol. A: Chem. 157 (2003) 55–63.
[6] J.C. Yu, J.G. Yu, W.K. Ho, Z.T. Jiang, L.Z. Zhang, Chem. Mater. 14 (2002) 3808–3816.
[7] D. Li, H. Haneda, S. Hishita, N. Ohashi, J. Solid State Chem. 178 (2005) 3293–3302.
[8] H. Luo, T. Takata, Y. Lee, K. Domen, J. Zhao, Y. Yan, Chem. Mater. 16 (2004) 846–849.
[9] X.Z. Li, H.L. Liu, P.T. Yue, Y.P. Sun, Environ. Sci. Technol. 34 (2000) 4401–4405.
[10] H. Hidaka, K. Ajisaka, S. Horikoshi, T. Oyama, K. Takeuchi, J. Zhao, N. Serpone, J. Photochem. Photobiol. A: Chem. 138 (2001) 185–192.
[11] K. Vinodgopal, I. Bedja, P.V. Kamat, Chem. Mater. 8 (1996) 2180–2187.
[12] H. Hidaka, T. Shimura, K. Ajisaka, S. Horikoshi, J. Zhao, N. Serpone, J. Photochem. Photobiol. A: Chem. 109 (1997) 165–170.
[13] R.A. Caruso, J.H. Schattka, A. Greiner, Adv. Mater. 13 (2001) 1577–1579.
[14] D.L. Ma, L.S. Schadler, R.W. Siegel, J.-I.L. Hong, Appl. Phys. Lett. 83 (2003) 1839–1841.
[15] M. Adachi, Y. Murata, M. Harada, S. Yoshikawa, Chem. Lett. 8 (2000) 942–946.
[16] Y. Zhu, H. Li, Y. Koltypin, Y.R. Hacohen, A. Gedanken, Chem. Commun. 24 (2001), 2616–267.
[17] T. Kasuga, M. Hiramatsu, A. Hoson, T. Sekino, K. Niihara, Adv. Mater. 11 (1999) 1307–1311.
[18] G.H. Du, Q. Chen, R.C. Che, Z.Y. Yuan, L.M. Peng, Appl. Phys. Lett. 79 (2001) 3702–3705.
[19] V. Zwilling, M. Aucouturier, E. Darque-Ceretti, Electrochim. Acta 45 (1999) 921–929.
[20] O.K. Varghese, D. Gong, M. Paulose, C.A. Grimes, E.C. Dickey, J. Mater. Res. 18 (2003) 156–165.
[21] X. Quan, S.G. Yang, X.L. Ruan, H.M. Zhao, Environ. Sci. Technol. 39 (2005) 3770–3775.
[22] A. Ghicov, H. Tsuchiya, J.M. Macak, P. Schmuki, Electrochem. Commun. 7 (2005) 505–509.
[23] M. Paulose, K. Shankar, S. Yoriya, H.E. Prakasam, O.K. Varghese, G.K. Mor, T.A. Latempa, A. Fitzgerald, C.A. Grimes, J. Phys. Chem. B 110 (2006) 16179–16184.
[24] R.P. Vitiello, J.M. Macak, A. Ghicov, H. Tsuchiya, L.F.P. Dick, P. Schmuki, Electrochem. Commun. 8 (2006) 544–548.

[25] A. Ghicov, J.M. Macak, H. Tsuchiya, J. Kunze, V. Haeublein, L. Frey, P. Schmuki, Nano Lett. 6 (2006) 1080–1082.
[26] J.M. Macak, H. Tsuchiya, P. Schmuki, Angew. Chem. Int. Ed. 44 (2005) 2100–2102.
[27] K. Zhu, N.R. Neale, A. Miedaner, A.J. Frank, Nano Lett. 7 (2007) 69–74.
[28] H. Masuda, K. Fukuda, Science 268 (1995) 1466–1468.
[29] Y.K. Lai, L. Sun, C. Chen, C.G. Nie, J. Zuo, C.J. Lin, Appl. Surf. Sci. 252 (2005) 1101–1106.
[30] S. Sakthivel, H. Kisch, Angew. Chem. Int. Ed. 42 (2003) 4908–4911.
[31] R. Asahi, T. Morikawa, T. Ohwaki, K. Aoki, Y. Taga, Science 293 (2001) 269–271.
[32] C. Minero, G. Mariella, V. Maurino, D. Vione, E. Pelizzetti, Langmuir 16 (2000) 8694–8972.
[33] C. Minero, G. Mariella, V. Maurino, E. Pelizzetti, Langmuir 16 (2000) 2636–2641.
[34] R. Sanjines, H. Tang, H. Berger, F. Gozzo, G. Margaritondo, F. Lévy, J. Appl. Phys. 75 (1994) 2945–2951.
[35] Z.L. Liu, B. Guo, L. Hong, H.X. Jiang, J. Phys. Chem. Solids 66 (2005) 161–167.
[36] A. Bensalem, F. Bozon-Verduraz, M. Delamar, G. Bugli, Appl. Catal. A: Gen. 121 (1995) 81–93.
[37] Y.K. Lai, L. Sun, J. Zuo, C.J. Lin, Acta Phys. Chim. Sin. 20 (2004) 1063–1066.
[38] Q.Y. Cai, M. Paulose, O.K. Varghese, C.A. Grimes, J. Mater. Res. 20 (2005) 230–236.
[39] M.R. Hoffmann, S.T. Martin, W.Y. Choi, D.W. Bahnemannt, Chem. Rev. 95 (1995) 69–96.
[40] S. Chih-Cheng, C. Tse-Chuan, J. Mol. Catal. A: Chem. 151 (2000) 133–145.
[41] W.H. Leng, Z. Zhang, J.Q. Zhang, J. Mol. Catal. A: Chem. 206 (2003) 239–252.
[42] X.Z. Li, H.L. Liu, P.T. Yue, Y.P. Sun, Environ. Sci. Technol. 34 (2000) 4401–4406.
[43] T.C. An, Y. Xiong, G.Y. Li, C.H. Zha, X.H. Zhu, J. Photochem. Photobiol. A: Chem. 152 (2002) 155–165.